Fishbone instability driven by trapped fast ions in a toroidal plasma with reversed magnetic shear

Original
Fishbone instability driven by trapped fast ions in a toroidal plasma with reversed magnetic shear / Miao, Y., Hao, G.Z., He, H.D., Hole, M.J., Porcelli, F., Qu, Z.S., Liu, Y., Wang, S., Dong, G.Q., Chen, W., Chen, H.T., Wang, Y.Q., Gao, Q.D., Wang, A.K., Xu, M.. - In: NUCLEAR FUSION. - ISSN 0029-5515. - 60:9(2020), p. 096022. [10.1088/1741-4326/aba1ce]

Publisher:
IOP Publishing Ltd

Published
DOI:10.1088/1741-4326/aba1ce

ACCEPTED MANUSCRIPT

Fishbone instability driven by trapped fast ions in a toroidal plasma with reversed magnetic shear

To cite this article before publication: Yutian Miao *et al* 2020 *Nucl. Fusion* in press https://doi.org/10.1088/1741-4326/aba1ce

Manuscript version: Accepted Manuscript

Accepted Manuscript is “the version of the article accepted for publication including all changes made as a result of the peer review process, and which may also include the addition to the article by IOP Publishing of a header, an article ID, a cover sheet and/or an ‘Accepted Manuscript’ watermark, but excluding any other editing, typesetting or other changes made by IOP Publishing and/or its licensors”

This Accepted Manuscript is © **2020 IAEA, Vienna**.

During the embargo period (the 12 month period from the publication of the Version of Record of this article), the Accepted Manuscript is fully protected by copyright and cannot be reused or reposted elsewhere.
As the Version of Record of this article is going to be / has been published on a subscription basis, this Accepted Manuscript is available for reuse under a CC BY-NC-ND 3.0 licence after the 12 month embargo period.

After the embargo period, everyone is permitted to use copy and redistribute this article for non-commercial purposes only, provided that they adhere to all the terms of the licence https://creativecommons.org/licences/by-nc-nd/3.0

Although reasonable endeavours have been taken to obtain all necessary permissions from third parties to include their copyrighted content within this article, their full citation and copyright line may not be present in this Accepted Manuscript version. Before using any content from this article, please refer to the Version of Record on IOPscience once published for full citation and copyright details, as permissions will likely be required. All third party content is fully copyright protected, unless specifically stated otherwise in the figure caption in the Version of Record.

View the article online for updates and enhancements.

This content was downloaded from IP address 134.117.10.200 on 17/07/2020 at 05:49

Fishbone instability driven by trapped fast ions in a toroidal plasma with reversed magnetic shear

Y.T. Miao[1,2], G.Z. Hao[2a], H.D. He[2], M.J.Hole[3], F.Porcelli[4], Z.S. Qu[3],Yue Liu[1], S. Wang[2], G.Q. Dong[2], W. Chen[2], H.T. Chen[2], Y.Q. Wang[2], Q.D. Gao[2], A.K. Wang[2] and M. Xu[2]

[1]*Key Laboratory of Materials Modification by Laser,*
Ion and Electron Beams, Ministry of Education,
School of Physics and Optoelectronic Technology,
Dalian University of Technology, Dalian 116024, China
[2]*Southwestern Institute of Physics, Chengdu 610041, China*
[3] *Australian National University, Acton 0200, ACT Australia*
[4] *Polytechnic University of Turin,Torino 10129 , Italy*

(Dated: June 1, 2020)

Abstract

Based on the non-perturbative approach, the hybrid code MARS-K is applied to study fishbone (FB) instabilities driven by trapped fast ions in a toroidal plasma with q profile nearly being flat or non-monotonic. We explore the dependency of the fishbone with variation in the fast ion distribution, thermal particle kinetic effects, safety factor (q) profile and plasma resistivity. When the safety factor minimum value is larger than unity (i.e. $q_{min} > 1$), the mode can be excited by isotropic or anisotropic fast ions, with the latter strongly enhancing the mode growth rate. The mode frequency increases with increasing q_{min}, and is more easily triggered in a equilibrium with two $q = 1$ surfaces, compared with the case with one or no $q = 1$ surface. Kinetic contributions from transit resonance of passing fast ions and from bounce resonance of trapped fast ions strongly enhance mode instability. The passing thermal ions induced Landau damping has a strong stabilization effect. Furthermore, in such a weak, even reversed magnetic shear plasma, the radial mode structure of fishbone mode monotonically decreases to zero at $q = 1$ flux surface instead of a step-like function, and it depends on the kinetic contributions from particles. In addition, the plasma resistivity significantly stabilizes the mode near the marginally unstable point.

---

[a] haogz@swip.ac.cn

1. INTRODUCTION

In tokamaks, fast ions, generated by neutral beam injection (NBI), can significantly affect various kinds of magnetic-hydrodynamics (MHD) instabilities, such as resistive wall mode [1–3] and tearing mode [4]. Fast ions can trigger a variety of instabilities, such as Alfvén Eigenmodes [5, 6], the fishbone mode [7, 8], fishbone-like modes [9, 10] and peeling modes [11]. The fishbone instability also induces the transport and loss of fast ions, which in turn reduces the NBI heating efficiency and plasma performance.

The fishbone mode was firstly observed during perpendicular NBI on the Poloidal Divertor Experiment (PDX) device [12] in 1983. Since this time fishbone modes have been observed on many other devices, such as PBX [13], DIII-D [14–16], JET [17–24],JT-60U [25], EAST [26], HL-2A [27–29], NSTX [30] and MAST [31]. The study of fishbone instability is still one of the most active topics of research.

In analytical studies, some approximations are made in order to obtain the dispersion relation [7, 30, 32–35], such as assuming large aspect ratio, assuming a step mode structure, and neglecting the kinetic modification on the mode structure. In addition, the perturbed potential energy from bulk plasma is assumed to be fixed in analytical model.

However, recent experimental [36] and theoretical [37] studies have shown that fast ions have significant effect on the mode structure. The perturbed fluid potential energy, which plays a significant role on determining the fishbone growth rate based on variation principle [7, 32], should be self-consistently computed when the fishbone mode structure is modified by particle kinetic effects. NIMROD simulation results show that the fishbone mode structure is different from internal kink [38], in which the thermal particle kinetic effect is neglected and monotonic q profile is adopted.

In MAST, NSTX and HL-2A plasmas, a fishbone instability can be driven by fast ions in discharges with reversed magnetic shear in the core region [27, 31, 39]. The dependence of fishbone on the fast ion distribution, various resonances, and q profile [33, 34, 40] requires more numerical investigations. Here, we apply the well benchmarked MHD-hybrid code MARS-K [41, 42] to study the above effects on fishbone, with self-consistent treatment of not only the eigenvalue but also the mode eigenfunction.

The work is structured as follows. Section 2 describes the formulation of MHD-kinetic hybrid model and the fast ion distribution function. Section 3 reports the numerical results showing the influence of fast ion anisotropy, thermal particles, q profile and plasma resistivity on fishbone instability eigenvalue and mode structure. A summary and discussion are presented in Sec.4

2. MARS-K CODE

In this work, the MHD-kinetic hybrid code MARS-K is employed [41]. The kinetic effect from various particle species is evaluated by the solution of the linearized drift kinetic equation

[43].

For the equilibrium distribution function of fast ions $\hat{f}_h^0$, we assume a slowing down distribution function in energy space with a Gaussian one in pitch space [2] as shown below.

$$\hat{f}_h^0(\psi_p, \varepsilon, \chi) = \frac{C(\psi_p)}{\varepsilon_k^{3/2} + \varepsilon_c^{3/2}} \frac{1}{2\sqrt{\pi}\delta\chi} \sum_i C_i \exp\left[-\frac{(\chi - \chi_i)^2}{\delta\chi^2}\right], \tag{1}$$

where ε_a is the birth energy of fast ions, and $\varepsilon_c = (\frac{3\sqrt{\pi}}{4})^{2/3}(\frac{M_h}{M_i})(\frac{M_i}{M_e})^{1/3}T_e$ is the cut-off energy of fast ions. Here, the Gaussian width $\delta\chi$ weakly depends on the particle energy ε_k, which is written as

$$\delta\chi^2(\psi, \varepsilon) = \delta\chi_0^2 - \frac{1}{3}\ln\left[\frac{\varepsilon_k^{3/2}\left(1 + \varepsilon_c^{3/2}/\varepsilon_a^{3/2}\right)}{\varepsilon_k^{3/2} + \varepsilon_c^{3/2}}\right]. \tag{2}$$

In MARS-K, a curvilinear flux coordinate system (s, θ, ϕ) is employed, such that $s \equiv \sqrt{\psi_p}$, with ψ_p being the poloidal flux, and θ and ϕ are the general poloidal and toroidal angle, respectively. The function $C(\psi_p)$ is a function of poloidal flux, describing the dependence of fast ion density on the radial coordinate. The coefficients C_i and χ_i describe fast ion distribution in pitch space [2, 44], $\chi = v_\parallel/v$ is defined as the pitch of fast ion, and $\delta\chi_0$ is the parameter we will scan below, which is referred to as the Gaussian width in pitch space for the fast ions with birth energy. Theoretically, as $\delta\chi \to \infty$, the anisotropic distribution model recovers to the isotropic model. MARS-K has two separate implementations for the anisotropic and isotropic models, which allows the internal benchmarks between these two models.

3. NUMERICAL RESULTS

A. Equilibrium

In this work, we choose a toroidal plasma with large aspect ratio (i.e., $\epsilon = a/R_0 = 0.36/1.65 \simeq 0.2$). The toroidal magnetic field at axis is $B_0 = 1.3$ T, the central electron density $n_e(0) = 1.38 \times 10^{19}$ m^{-3}, and we assume that the electron temperature equals to that of ions ($i.e. T_e(0) = T_i(0) = 1.5$ keV). The above parameters are reasonable for the discharges on the HL-2A device [45]. Figure 1 (a) plots the normalized pressure profile. Figure 1 (b) shows the safety factor profile with reversed magnetic shear in the core region. There are three rational surfaces inside plasma for this case. When minimum of q ($i.e.$ q_{min}) is scanned as studied in Sec.(3 C), there may be only one or two rational surfaces inside the plasma. Figure 1 (c) and (d) display the fast ion pressure and density profiles normalized to the thermal pressure and electron density, respectively. In our calculation, electron density is equal to total ion density, including both the thermal and fast ions.

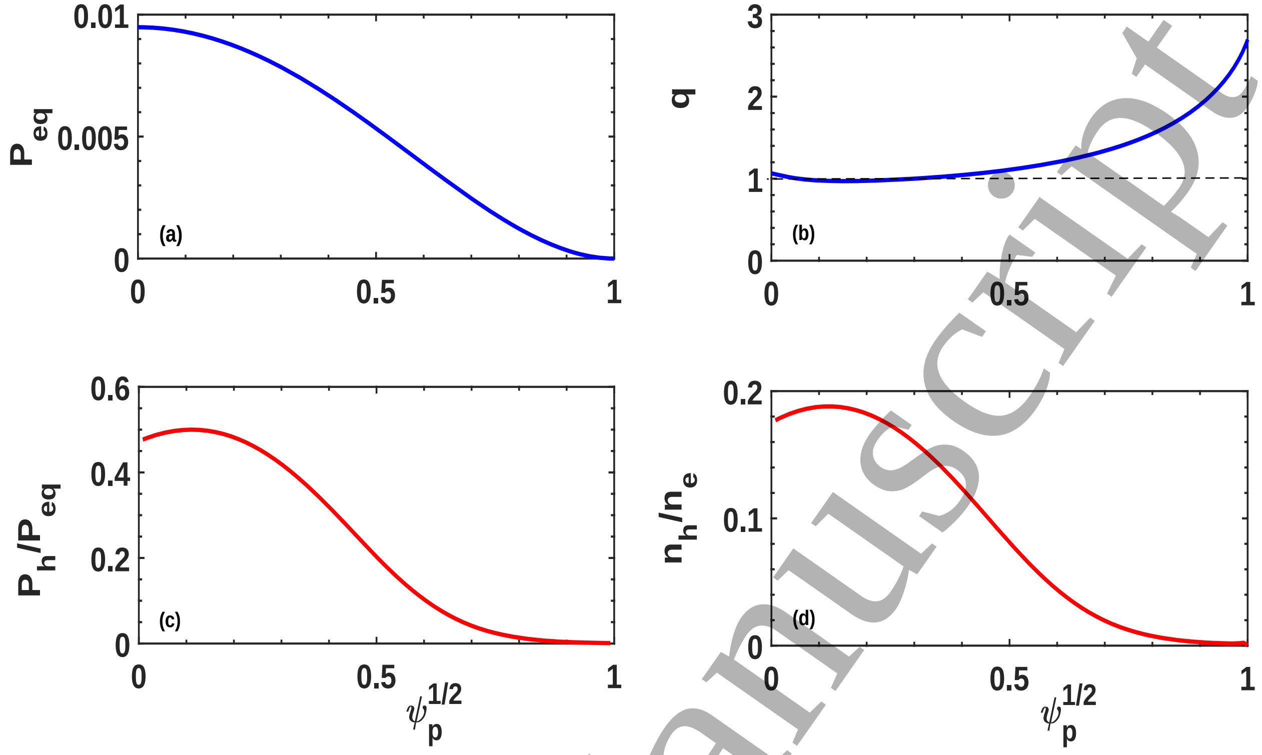

FIG. 1. Equilibrium reference case radial profiles. (a) Pressure normalized by B_0^2/μ_0 with $\beta_N = 1.158$; (b) safety factor q with reversed magnetic shear in the core region ($q_{min} = 0.97$); (c) ratio of fast ion pressure (P_h) to total plasma pressure (P_{eq}); (d) ratio of fast ion density (n_h) to electron density (n_e). Horizontal dashed line in (b) denotes $q = 1$ value.

B. Effect of fast ion distribution on fishbone instability

In theory, it has been shown that both the growth rate and frequency of fishbone depend on the fast ion distribution function [33, 34]. Here, we linearly study the fishbone driven by trapped fast ions and its dependence on fast ion distribution function, including the kinetic effect of fast ions on the mode structure [41]. In the figures below, the growth rate and frequency are normalized by the Alfvén frequency (ω_A) computed at the magnetic axis.

Figure 2 shows linear properties of the fishbone mode for the equilibrium of Fig. 1. Figure 2 (a) shows that the birth energy of fast ions is almost 45 keV in the whole plasma region. Figure 2 (b) displays the averaged toroidal precession drift frequency (ω_d) of trapped fast ions, which is in the order of 10^{-2} at the position where $q \sim 1$. Here, only the non-adiabatic contribution from trapped fast ions is included, in addition to the adiabatic contributions from all species. Figure 2(c) indicates that the mode growth rate strongly depends on the Gaussian width parameter $\delta\chi_0$ in the region $0 < \delta\chi_0 < 1.5$. The growth rate γ/ω_A decreases from 0.08 to 0.02 as $\delta\chi_0$ varies from 0.25 to 1.5. The corresponding mode frequency ω_r/ω_A decreases from 0.05 to 0.035. When $\delta\chi_0 > 1.5$, the eigenvalue from anisotropic model agrees well with that from isotropic model. This also numerically confirms the results from anisotropic model. For the Toroidal-Alfvén-Eigenmode driven by fast ions, similar results were obtained [46].

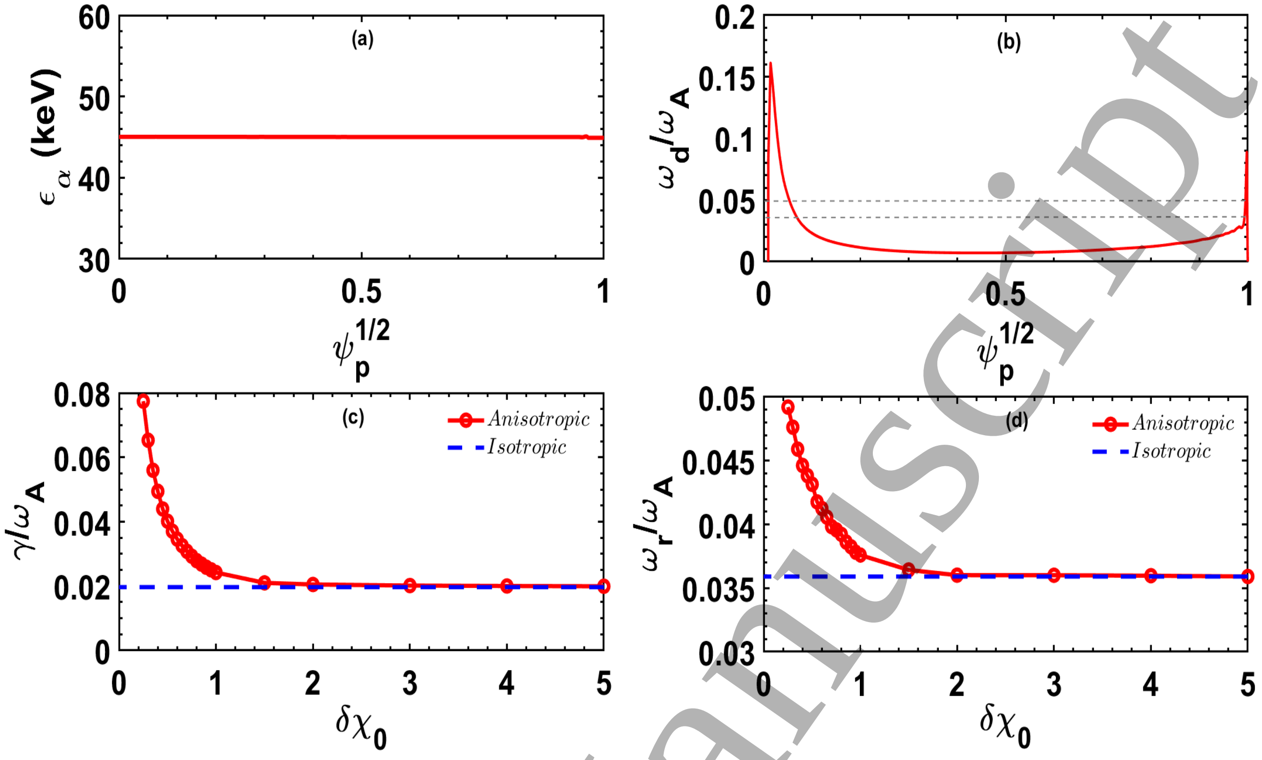

FIG. 2. Linear properties of the fishbone mode for the equilibrium of Fig. 1. Radial profile of (a) fast ion birth energy, (b) toroidal precession drift frequency averaged over the velocity space. The normalized growth rate (c) and real frequency (d) versus the Gaussian width parameter $\delta\chi_0$ (red circle curve). In (b), two horizontal lines denote the maximum and minimum value of mode frequency shown in (d). The eigenvalue obtained by isotropic model is also presented (dashed curves in (c) and (d)). In the non-adiabatic parts, only the precessional resonance from trapped fast ions is included.

It is pointed out that, here, a decrease of $\delta\chi_0$ (keeping fast ion pressure as done in Fig.2) implies an increase in the fraction of trapped fast ions, and roughly corresponds to the increase of fast ion pressure with the fixed $\delta\chi_0$. Hence, when $\delta\chi_0$ decreases, the fishbone growth rate is enhanced. The mode frequency also increases with increasing driving (i.e. a decrease of $\delta\chi_0$). The order of mode frequency is mainly determined by the resonance condition $\omega_r = \omega_d$, here, since no plasma rotation is assumed. The mode frequency is comparable to ω_d in the core region (Fig.2 (b)). Here, the dominant component for fishbone is $m/n = 1/1$. Furthermore, we find the amplitude of fishbone growth rate is comparable with the mode frequency. The above results are consistent with the results predicted by NIMROD code [38].

C. Effect of q profile and q_{min} on fishbone instability

Recent analytical results show that the fishbone (FB) instability driven by passing fast ions is sensitive to the safety factor profile. The higher the magnetic shear, the larger threshold of fast ion pressure required to drive the fishbone [33]. In this work we numerically study the dependence of the fishbone on the q profile using the non-perturbative approach. Figure 3 compares results for the fishbone and internal kink mode. Four cases with different q profiles are considered as shown in Fig.3(a). For the magnetic shear, the main difference exists in the region $\sqrt{\psi_p} < 0.3$ (Fig.3(b)). In order to exclude the influence of fishbone eigenvalue by plasma pressure we have set the normalized plasma beta to be the same in these cases.

Here, for the convenient of discussing the numerical results, the perturbed kinetic energy from particles δW_K is introduced and written as $\delta W_K = \sum_{j=i,e,h} \delta W_K^{a,j} + \alpha_D \delta W_K^{na,NTD,h}$, with α_D a multiplier for the non-adiabatic contribution from the precession resonance of trapped fast ions. The subscript $j = i, e$, and h denote thermal ions, thermal electrons and fast ions, respectively. The superscript 'a' and 'na' denote the adiabatic and non-adiabatic contribution (also called kinetic effect) from each kind of species. The superscript 'NTD' stands for Non-adiabatic contribution from the Toroidal precession Drift resonance of trapped particle. Figure 3(c) shows that the internal kink (IK) instability is fully stabilized as α_D exceeds a critical value. Meanwhile, when α_D is larger than a threshold $\alpha_{D,c}$, fishbone instability is excited. For the studied four cases, $\alpha_{D,c}$ is equal to 0.15, 0.2, 0.22, and 0.59, respectively. Comparison between cases 2 and 4 shows that the threshold value $\alpha_{D,c}$ is insensitive to magnetic shear in the core region. Comparisons of cases 1, 2 and 3 indicate that the $\alpha_{D,c}$ value is sensitive to the number of $q = 1$ surfaces. Comparison between cases 1 and 3 shows that, for the case without $q = 1$ surface, the $\alpha_{D,c}$ value is much larger than that including two $q = 1$ surfaces. The possible reason may be that the resonance between the mode and particles increases with an increasing number of resonant surfaces.

Figure 3(d) indicates that the fishbone real frequency is basically much larger than that of the internal kink. For case 3, however, there is a narrow region ($0.15 < \alpha_D < 0.2$), where both the fishbone and internal kink coexist, and the internal kink real frequency is very close to that of the fishbone. The branch bifurcation and mode transform occurs near the cross point as discussed in Ref. [47].

It is known (see in Refs. [48] and [49]) that reversed-shear q profiles of the type considered in this article can be ideal MHD unstable to $m/n = 1$ internal kink modes, even with zero plasma beta. The relevant threshold condition depends on the actual value of q_{min} and on details of the q profile. However, the $m/n = 1$ fishbone destabilized by energetic ions and the $m/n = 1$ internal kink,leading to sawtooth crashes (we shall refer to this branch of the m/n = 1 dispersion relation simply as sawtooth mode), are two different modes, their differences being reflected in their mode structures and threshold conditions. In this article, we focus our attention on the fishbone mode, while a detailed comparison between our numerical results and the theory of $m/n = 1$ sawtooth mode in plasmas with weak or reversed shear [48, 49] is beyond the scope of the present work.

In addition, the unstable n/m=1/1 sawtooth mode is almost static in plasma frame and has very small real frequency when the kinetic effect from particles is included. However, the fishbone is triggered by the wave-particle resonance, with its frequency being comparable

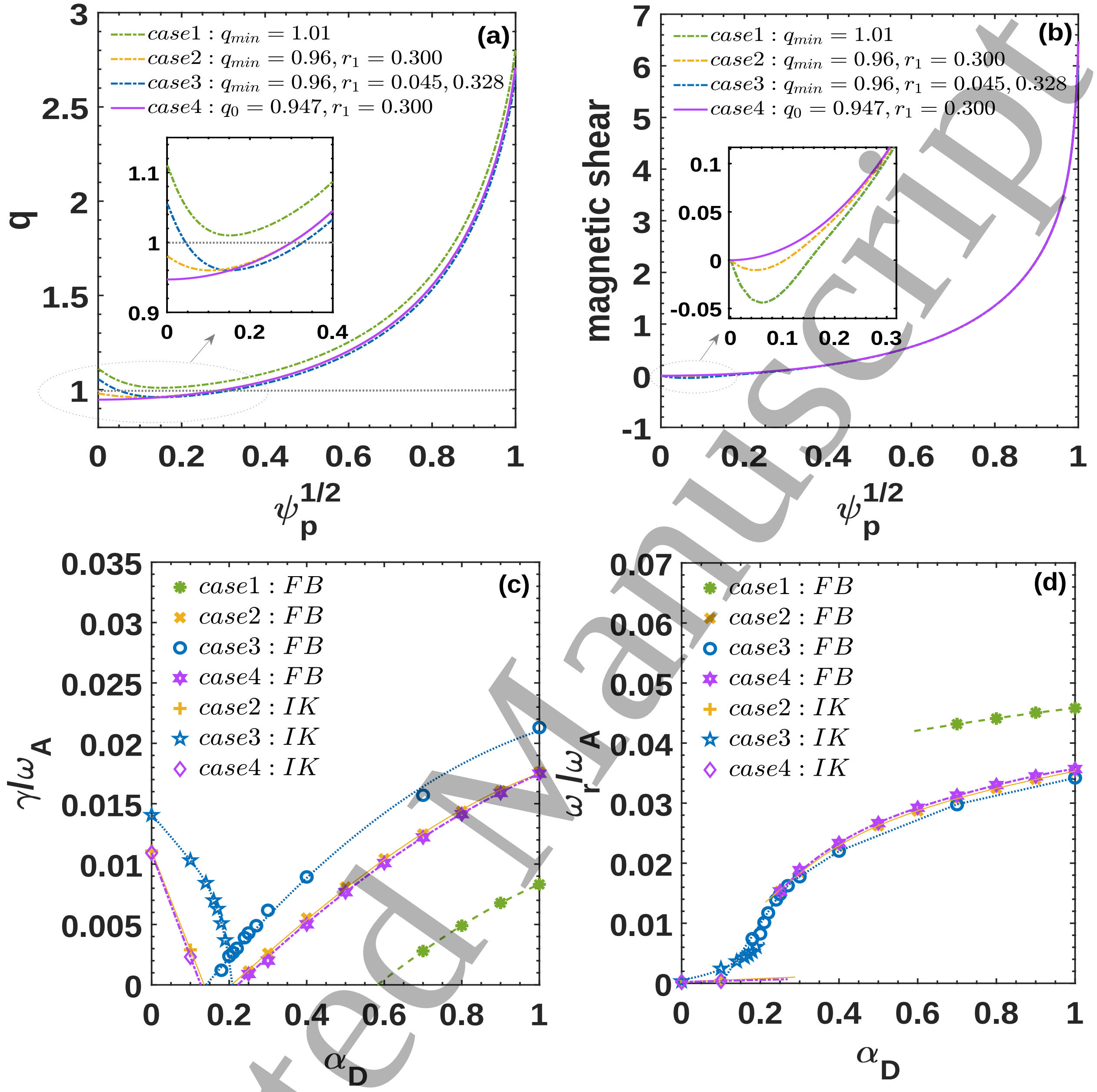

FIG. 3. Comparison of fishbone and internal kink frequency and growth rate for reversed-shear and monotonic q profiles. Radial profiles of (a) non-monotonic (reversed) and monotonic safety factor and (b) the corresponding magnetic shear. Plots (c) and (d) show the growth rate and real frequency of fishbone and internal kink instabilities for different q profiles, respectively. As a function of scaling factor α_D for non-adiabatic contribution of trapped particles (see main text). Here, isotropic model for fast ions is used.

with the precession drift frequency of trapped fast ions in this work. It is also known that fast ions can destabilize the fishbone mode, but they can also suppress the sawtooth mode. As we pointed out, the two modes have different stability thresholds. In our simulations, the regimes and equilibrium profiles of interest are such that the sawtooth mode is stable, while

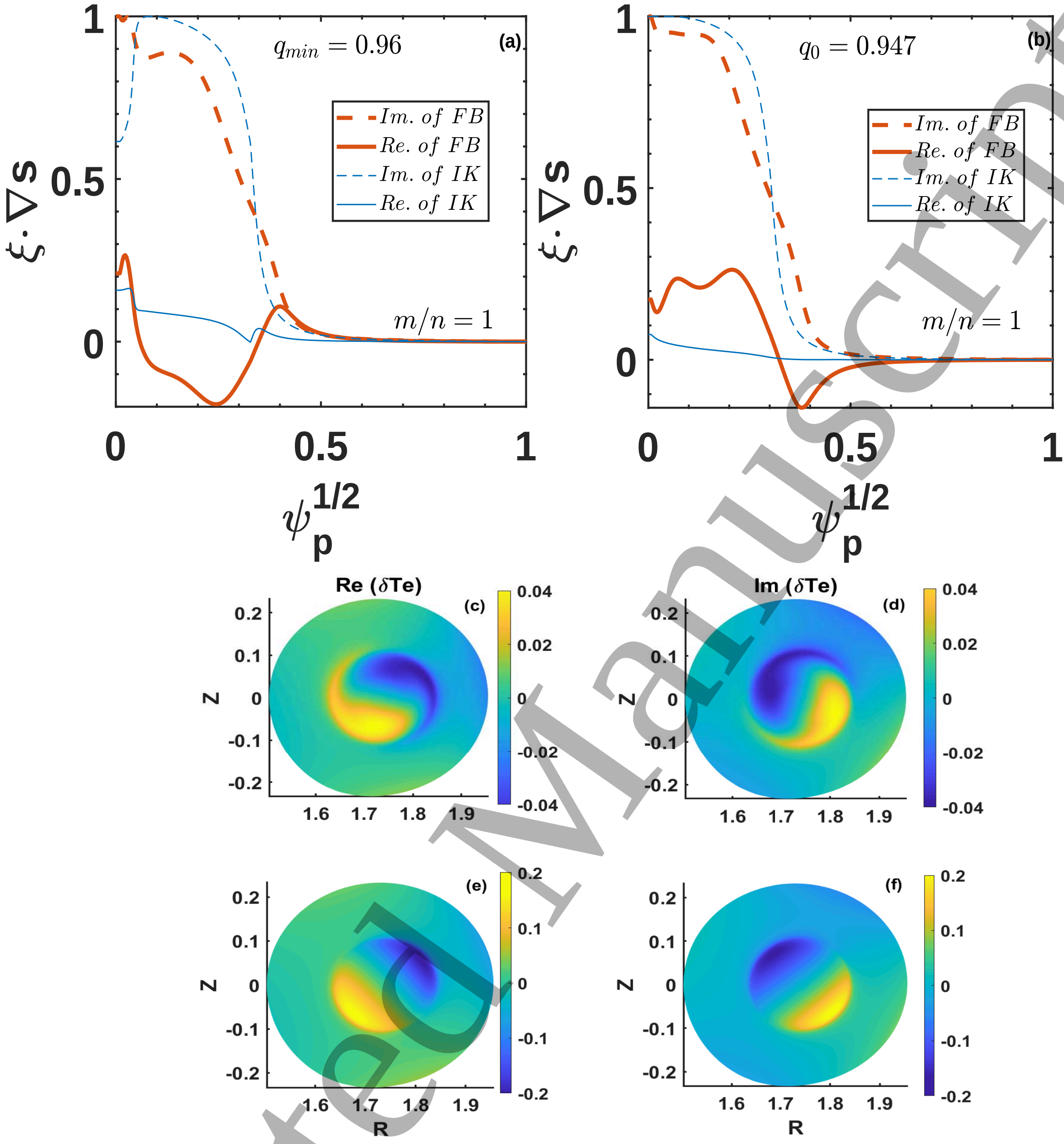

FIG. 4. Comparison of fishbone and internal kink displacements. Panels (a) and (b) plot the displacement of fishbone and internal kink instabilities for the two chosen q profiles (i.e. cases 3 and 4 respectively in Fig.3) (a). Panels (c) and (d) show real and imaginary parts of contour plot of perturbed temperature induced by the fishbone in the non-monotonic q profile. Here, δT_e is estimated based on the formula $\delta T_e = \boldsymbol{\xi} \cdot \nabla T_e$. Panels (e) and (f) present the 2D plot of δT_e induced by the internal kink.

the fishbone mode is driven unstable by the energetic ions. Clearly, in a real experiment, as core plasma profiles evolve in time, the sawtooth mode may become unstable.

Figure 4 shows the mode structure of internal kink and fishbone instabilities for cases 3 and 4 shown in Fig.3. Clearly, the profile of radial displacement ($\boldsymbol{\xi} \cdot \nabla s$) of the fishbone differs to that of the internal kink: $Im(\boldsymbol{\xi}\cdot\nabla s)$ of the internal kink is sharper near the rational surface, while $Re(\boldsymbol{\xi}\cdot\nabla s)$ of the fishbone is larger than that of internal kink, due to the kinetic contribution of fast ions. In addition, for the internal kink, $Im(\boldsymbol{\xi}\cdot\nabla s)$ has a drop near the axis for the reversed shear case, as expected. For the reversed shear case, the mode structures (in term of δT_e) of the fishbone and internal kink are contour plotted in the (R, Z) plane in Figs.4 (c)-(d) and (e)-(f), respectively. The fishbone mode structure is twisted and has a tail in the poloidal direction. This twist is induced by wave-particle resonance Ref. [37, 38]. However, the internal kink mode structure is not twisted. Here, 2D contour plot of δT_e supplies the possibility of direct comparison between computations and experimental measurements obtained by Electron Cyclotron Emission Image (ECEI) diagnostics.

Fishbone instabilities are experimentally observed in discharges with reversed magnetic shear and $q_{min} >\sim 1$ in various devices, such as HL-2A [50], MAST [51] and NSTX [52]. In addition, for the 9MA steady state ITER scenario, the magnetic shear is reversed in the core region and has a broad low value in the middle region [2, 53]. This motivates a study of the dependence of the fishbone on q_{min} for the reversed magnetic shear equilibrium.

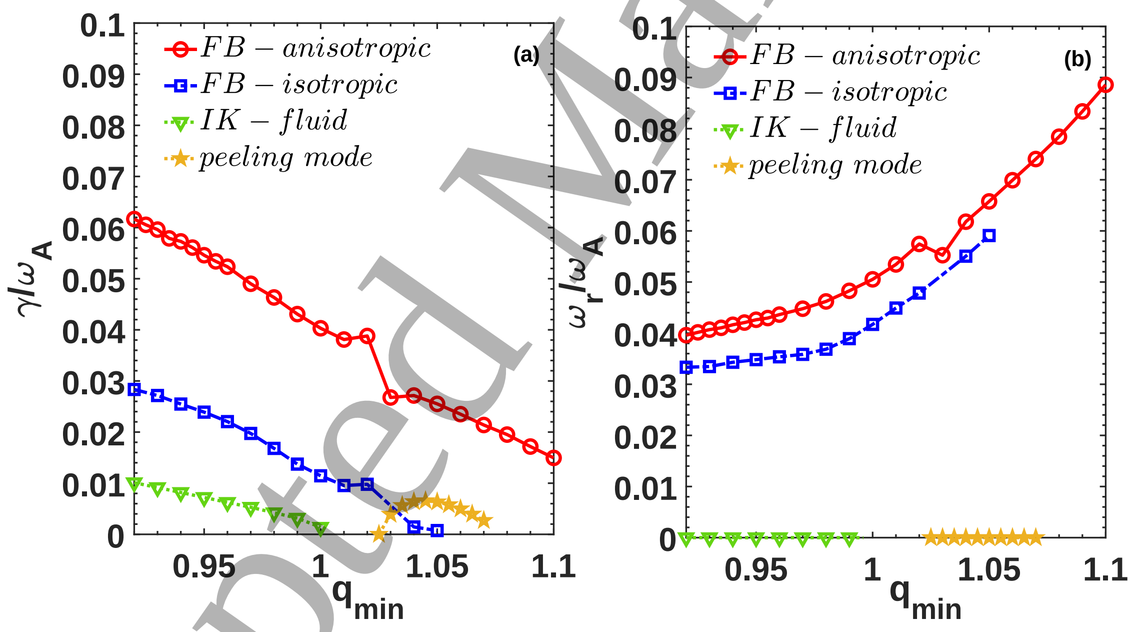

FIG. 5. Normalized growth rate (a) and real frequency (b) of fishbone and internal kink instabilities versus q_{min}. Blue (square) and red (circle) curves denote the cases of isotropic and anisotropic (with $\delta\chi_0 = 0.4$) fast ion models, respectively. Green (triangle) and Yellow (pentagram) curves display the cases of internal kink and peeling mode, respectively. During the scan of q_{min} value, the q profile and plasma pressure are fixed as given in Sec.3 A

.

Figure 5 presents the dependence of the fishbone eigenvalue on q_{min}. Figure 5 (a) shows two kink instabilities (internal kink and peeling mode) and two fishbone instabilities. As expected, the $m/n = 1/1$ internal kink is unstable when $q_{min} < 1$. Here, the ideal internal kink with $q_{min} < 1$ in a toroidal plasma is driven by the poloidal beta [54]. During the scan of q_{min}, an unstable peeling mode with dominant $m/n = 3/1$ appears in the window $1.03 < q_{min} < 1.07$, in which the safety factor at edge varies from 2.86 to 2.98. The internal kink is fully stabilized as the kinetic contribution of trapped fast ions is included. In contrast, the fishbone is excited by trapped fast ions.

For both isotropic and anisotropic cases, the fishbone growth rate decreases as q_{min} increases. The growth rate has a large variation near $q_{min} \sim 1.03$, which is related to the onset of unstable peeling modes. For the isotropic case, a fishbone mode is found for values of q in the interval $1 < q_{min} < 1.05$. For the anisotropic case, the fishbone growth rate is strongly enhanced in the whole q_{min} region. Meanwhile, the fishbone can exist in the $q_{min} > 1$ region, and the dependence of the fishbone growth rate on q_{min} is similar to that obtained by M3D-K code [40]. Figure 5 (b) indicates that the mode frequency (ω_r/ω_A) decreases from ~ 0.09 to ~ 0.04 as q_{min} decreases from 1.1 to 0.92. Hence, the variation of the fishbone frequency may be an indicator of the evolution of q_{min}. However, it should be noted that we did not consider the ion diamagnetic effect in our model. The 'diamagnetic' fishbone is thought to be related to the long-lived mode observed in experiments [55].

D. Effect of various drift energy components on fishbone instability

In MARS-K, the contribution induced by different kinds of particle motions (toroidal precession drift (NTD), bounce (NTB) and transit motions (NP)) can also be separately controlled. This allows MARS-K to investigate the combined effects of various kinds of kinetic contributions on the instabilities [2].

In this section, we mainly study the effect of thermal ions on fishbone instability. Two groups are considered as shown in Fig.6. One group only includes fast ion kinetic contribution. The other one includes both fast ions and thermal particles. In these two groups, the adiabatic part of both fast ions and thermal particles is included.

For the group without thermal particles, the transit and bounce resonances from passing and trapped fast ions, respectively, enhance the fishbone instability which is initially triggered by toroidal precession drift resonance from trapped fast ions. The fishbone growth rate increases from 0.05 for NTD to 0.104 for NTD+NP+NTB (Fig.6(a)). The real frequency increases as more fast ion kinetic contributions are included.

When all the thermal particle kinetic effects are added, the fishbone growth rate generally decreases. Especially, for the case labeled by NTD, the fishbone is almost fully suppressed by thermal particles.

For the case of NTD+NP and NTD+NP+NTB, the fishbone growth rate decreases from 0.08 to 0.06 and from 0.10 to 0.08, respectively, after including thermal particle kinetic effect. The stabilization of the fishbone by thermal particles is explained as the enhancement of Landau damping induced by the thermal particles.

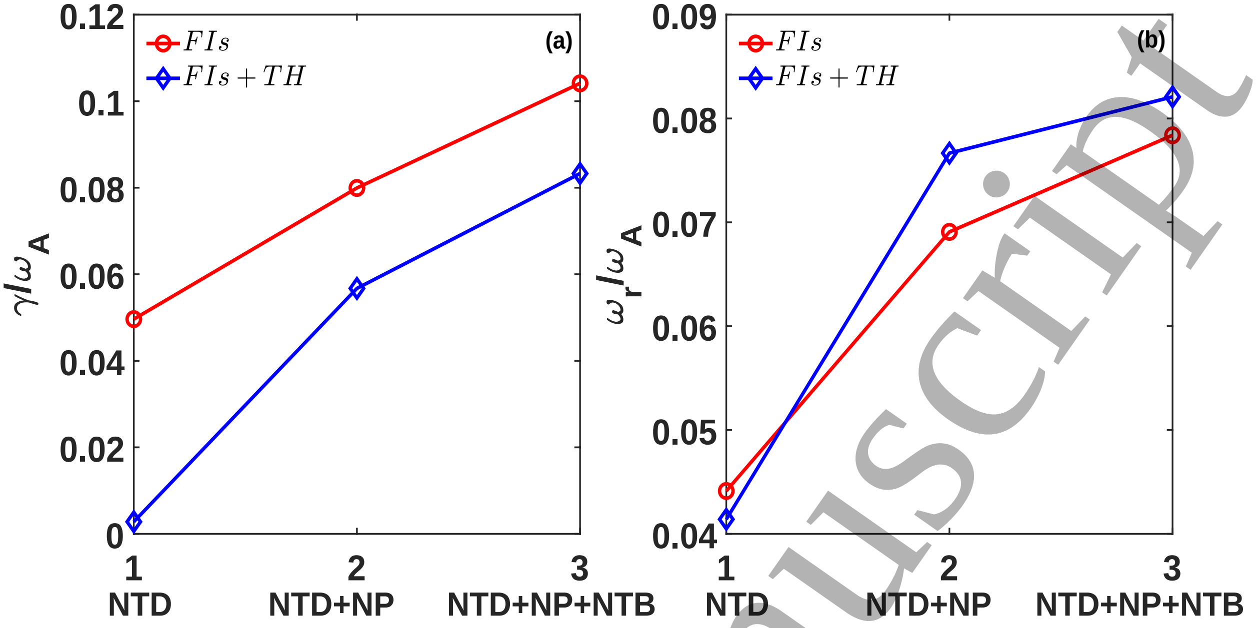

FIG. 6. Fishbone growth rate (a) and frequency (b) versus different kinetic contributions from fast ions (FIs) and thermal particles (TH), for the equilibrium given in Fig.1. Here, anisotropic model is adopted with $\delta\chi_0 = 0.4$. The terms NTD, NTB and NP stand for the non-adiabatic contribution from the Toroidal precession Drift resonance of trapped fast ions; the Non-adiabatic effect from Bounce resonance of Trapped particles and the Non-adiabatic contribution from transit resonances of passing particles, respectively.

Thermal particles slightly affect the fishbone real frequency (ω_r/ω_A). For the NTD case, ω_r/ω_A slightly decreases. While for the other two cases, ω_r/ω_A increases. However, thermal particle kinetic contributions do not change the trend of the dependence of ω_r/ω_A on the terms of fast ion kinetic contribution.

Figure 7 shows the mode structures corresponding to the eigenvalues shown in Fig.6. For the cases without thermal particle kinetic contributions (Fig.7 (a)-(c)), the peak position of the imaginary part of radial displacement ($\boldsymbol{\xi}\cdot\nabla s$) moves outwards from $\sqrt{\psi_p} = 0.08$ for the NTD case to $\sqrt{\psi_p} = 0.25$ for the NTD+NP+NTB case. The real part Re($\boldsymbol{\xi}\cdot\nabla s$) also depends on the terms of fast ion kinetic contributions.

For the case of NTD, Fig.7 (d) shows a significant modification of the fishbone mode structure by thermal particle kinetic effect, compared with that in Fig.7 (a). The mode tends to be localized in the $q \sim 1$ region. Figures 7 (e)-(f) indicate that the thermal particle kinetic contribution almost does not affect the mode structure which is mainly determined by fast ions, for the cases of NTD+NP and NTD+NP+NTB. Figures 6 and 7 reveal that thermal particle kinetic contributions not only affect the mode eigenvalue, but also have the remarkable influence on the mode structures when the mode eigenvalue has a large change.

It is interesting to note that the fishbone instability, obtained by the non-perturbative

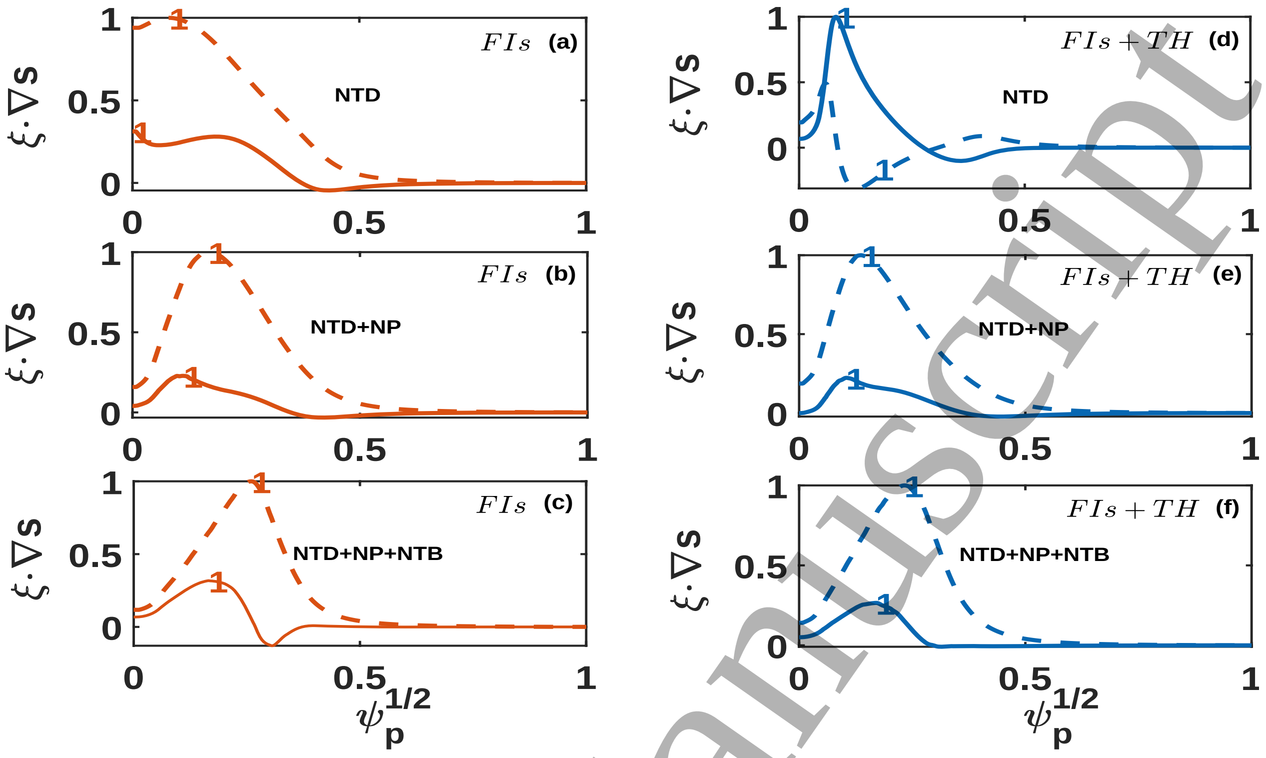

FIG. 7. Radial displacement of fishbone instabilities corresponding to the cases studied in Fig.6. Left column (i.e. (a) (b) and (c)) and right column(i.e. (d), (e) and (f)) denote the group without and with thermal particle kinetic effect, respectively. Real and imaginary parts of displacement are plotted by solid and dashed curves, respectively. For each case, $\boldsymbol{\xi}\cdot\nabla s$ is separately normalized by the maximum in $[Re(\boldsymbol{\xi}\cdot\nabla s), Im(\boldsymbol{\xi}\cdot\nabla s)]$.

approach, satisfies the general variation principle below.

$$\delta I + \delta W_{\rm MHD} + \delta W_K = 0, \tag{3}$$

where $\delta I = \frac{1}{2}(\gamma - i\omega_r)^2 \int d^3x\rho|\boldsymbol{\xi}_\perp|^2$ presents the inertial energy component, $\delta W_{\rm MHD}$ and δW_K refer to the perturbed MHD potential energy and the contributions from particles, respectively.

The dispersion relation in eq. (3) differs from the standard dispersion relation presented in Refs. [7, 8]. Indeed, in [7, 8], one finds $-i\omega \propto -\delta W$, while in our case $(-i\omega)^2 \propto -\delta W$ with $\omega = \omega_r + i\gamma$. The reason is that we considered in our simulations plasma equilibria with q profiles that are nearly flat, with very low and weakly reversed magnetic shear. For these profiles, the fishbone instability acquires nonstandard features. In particular, a transition layer at the $q = 1$ surface is no longer apparent in our numerical simulations, in the sense that the perturbed radial displacement, determined self-consistently including the modification by particle kinetic effects, does not look like the flat-top function that is typical of standard internal kink perturbations (note that, in the analytic works of Refs. [7, 8], the flat-top displacement is assumed, which implies that the plasma inertial term is mainly determined by the $q = 1$ transition layer, not present in our simulations). As far as we are aware, these nonstandard fishbone scenarios were first discussed in numerical simulation published in Ref. [56], while analytic work in support of the simulation of Ref. [56] was proposed, for instance, in Ref. [57].

The normalized version of Eq.(3) (by $\frac{1}{2}\int d^3x\rho|\boldsymbol{\xi}_\perp|^2$), is rewritten as,

$$\omega_r^2 - \gamma^2 = Re\left(\delta\hat{W}_{MHD} + \delta\hat{W}_K\right), \tag{4}$$

$$2\omega_r\gamma = Im\left(\delta\hat{W}_{MHD} + \delta\hat{W}_K\right). \tag{5}$$

Near the marginal point ($\omega_r >> \gamma >\sim 0$), Eqs. (4) and (5) imply a relation $\omega_r \sim \omega_d \simeq \sqrt{Re\left(\delta\hat{W}_{MHD} + \delta\hat{W}_K\right)}$, which determines a precessional fishbone with frequency ($\omega_r/\omega_A \simeq 0.03$) being comparable with that observed on HL-2A [58]. Further computations show that the fishbone driven by pure passing fast ions has a relatively larger frequency ($\omega_r/\omega_A \simeq 0.08$) determined by the transiting resonance ($\omega_r \sim \omega_t$) as expected. When the fishbone mode frequency is comparable with its growth rate (i.e. cases shown in Fig.6), the mode growth rate and real frequency is self-consistently determined by the general dispersion relation. For the 'diamagnetic' fishbone, its frequency satisfies $\omega_r \sim \omega_{*i} \sim \omega_d$ with ω_{*i} being the ion diamagnetic frequency, which is not considered in this work. Equations (4) and (5) are clearly verified by the MARS-K numerical simulation as shown in Fig.8, which shows the components. The term $\omega_r^2 - \gamma^2$ is exactly linearly propositional to $Re\left(\delta\hat{W}_{MHD} + \delta\hat{W}_K\right)$. Similarly, $2\omega_r\gamma$ linearly depends on $Im\left(\delta\hat{W}_{MHD} + \delta\hat{W}_K\right)$.

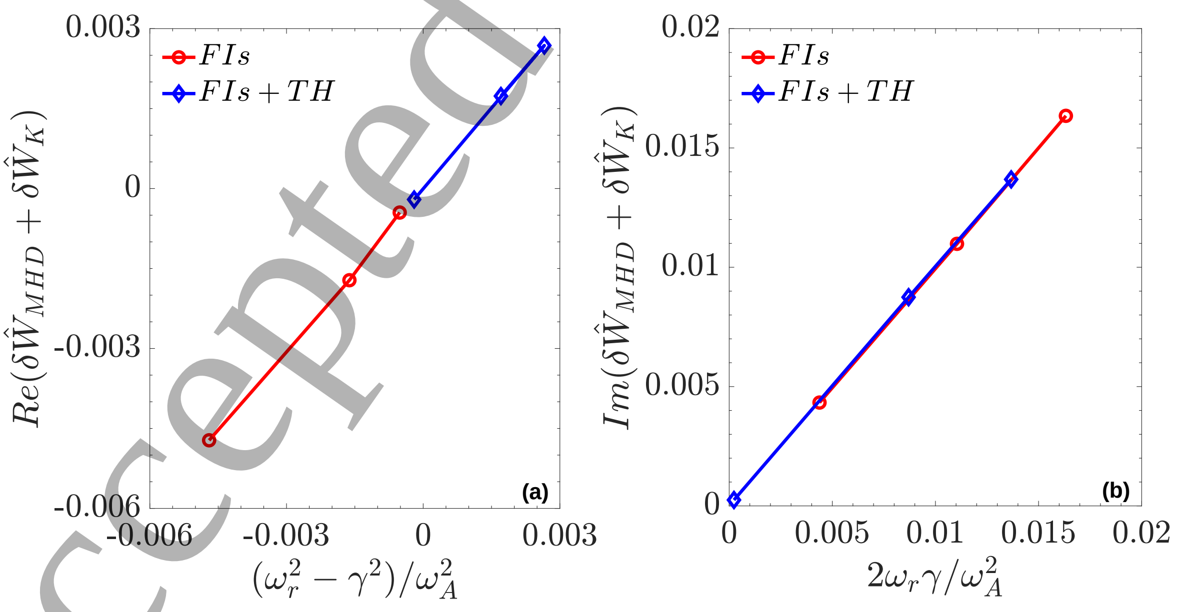

FIG. 8. The dependence of $(\omega_r^2 - \gamma^2)$(a) and $(2\gamma\omega_r)$(b) on the real and imaginary part of $\delta\hat{W}_{total} \equiv \delta\hat{W}_{MHD} + \delta\hat{W}_K$, corresponding to the results in Fig.6.

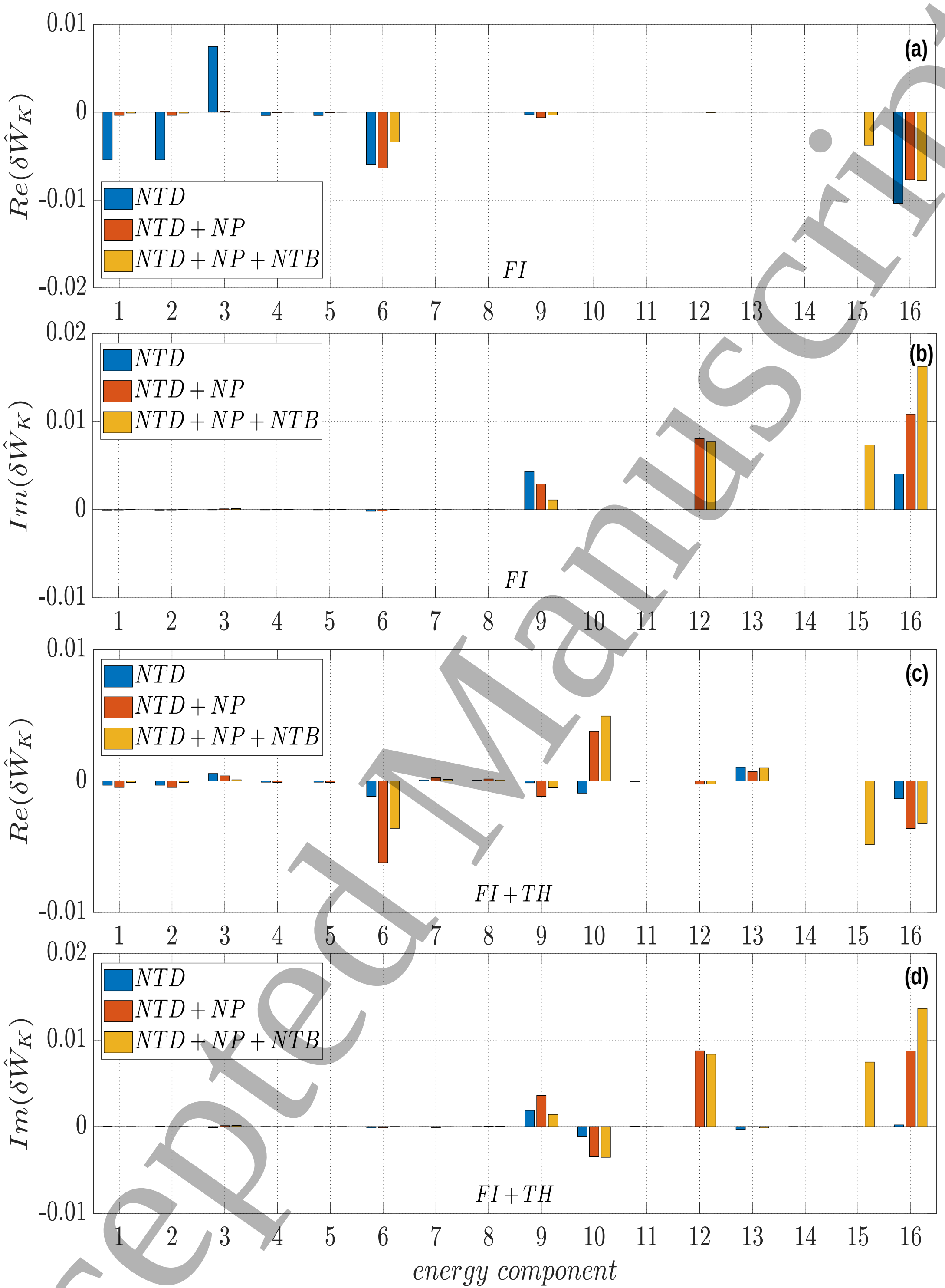

FIG. 9. Detailed perturbed energy components induced by particles for the perturbed energy $\delta \hat{W}_K$. Top row (i.e. (a) and (b)) and bottom row (i.e. (c) and (d)) correspond to the group without and with kinetic contributions from thermal particles, respectively. In each panel, integers along x-axis label the kind of contribution of the particles as described below. **1-3:** adiabatic part of passing thermal ions, electrons, fast ions; **4-6:** adiabatic part of trapped thermal ions, electrons, fast ions; **7-9:** non-adiabatic contribution from precession drift resonance of trapped thermal ions, electrons, fast ions (NTD); **10-12:** non-adiabatic contribution from transit resonance of passing thermal ions, electrons, fast ions (NP); **13-15:** non-adiabatic contribution from bounce resonance of trapped thermal ions, electrons, fast ions (NTB); **16:** summation over all the components.

The components of $\delta\hat{W}_K$ are plotted in Fig. 9 for the two groups studied in Fig.6. For the group without thermal particles, Figs. 9 (a) and (b) show that the real part of $\delta\hat{W}_K$ is mainly induced by the adiabatic contributions from particles, i.e.$Re(\delta\hat{W}_K) \simeq \sum_j Re(\delta\hat{W}_K^{a,j})$. For $Re(\delta\hat{W}_K)$, the adiabatic contributions from passing particles (all the three species) and trapped fast ions are dominant. Whilst the imaginary part $Im(\delta\hat{W}_K)$ mainly comes from the non-adiabatic contributions of fast ions, i.e. $Im(\delta\hat{W}_K) \simeq Im(\delta\hat{W}_K^{na,h})$. The contribution from transit resonance of passing fast ions or from the bounce resonance of trapped fast ions can significantly enhance the total $Im(\delta\hat{W}_K)$. The above two resonances are even stronger than the precession drift resonance. The study on the fishbone driven by pure transit resonance or pure bounce resonance will be carried out in future.

For the group including thermal particles, $Re(\delta\hat{W}_K)$ is mainly determined by adiabatic contribution of trapped fast ions and by the non-adiabatic effect of transit resonance of passing thermal ions and bounce resonance of trapped fast ions as shown in Fig.9(c). For the NTD case, the adiabatic contribution from particles is relatively reduced, compared with those shown in Fig.9 (a). It may be due to that the width of mode structure becomes narrower as the thermal particle kinetic effect is added (Fig.7 (d)), which significantly affects the adiabatic parts. Comparing with the group without thermal particles, for $Im(\delta\hat{W}_K)$, the contribution from transit resonance of passing thermal ions is remarkably enhanced and partly cancels the amplitude of kinetic contribution from fast ions. Finally, the passing thermal ions induces a remarkable decrease of total $Im(\delta\hat{W}_K)$. However, the FB frequency is insensitive to the thermal particle kinetic effect (Fig.6(b)), which implies $\gamma \propto Im(\delta\hat{W}_K)$ based on Eq.(5). Hence, the Landau damping induced by passing thermal ions plays the stabilizing role on the FB. For a direct comparison between modeling results and experimental observations, the careful inclusion of Landau damping is important.

E. Effect of plasma resistivity on fishbone

The experiments on ASDEX-U [59] show that $m/n = 1/1$ fishbones initiate $m/n = 3/2, 2/2$ neoclassical tearing mode (NTM) reconnection, which implies that the plasma resistivity plays a role in this phenomenon. An analytical model for resistive fishbone was derived in Ref. [60], including resistive layer inertia. However, in Ref. [60], only one rational ($q = 1$) surface is assumed and the continuum damping is ignored. Recent numerical results confirm that the resistivity stabilizes/destabilizes fishbone/internal-kink instabilities [61], respectively, in which only one rational surface is considered. In this section, we study the effect of resistivity on fishbone for the equilibrium with two rational surfaces given by 'case 4' in Fig.3(a).

For the chosen equilibrium, the estimated value of magnetic Reynolds number is $S \sim 5 \times 10^7$ ($S^{-1/3} = 2.7\times10^{-3}$) based on the parameters given in Sec. 3(A). The normalized electron skin depth d_e/r_1 and ion Larmor radius ρ_s/r_1 are 1.5×10^{-3} and 5.5×10^{-2}, respectively. Here, $r_1 \sim 0.1$ m is the radial position of $q = 1$ surface. The parameters satisfy inequalities

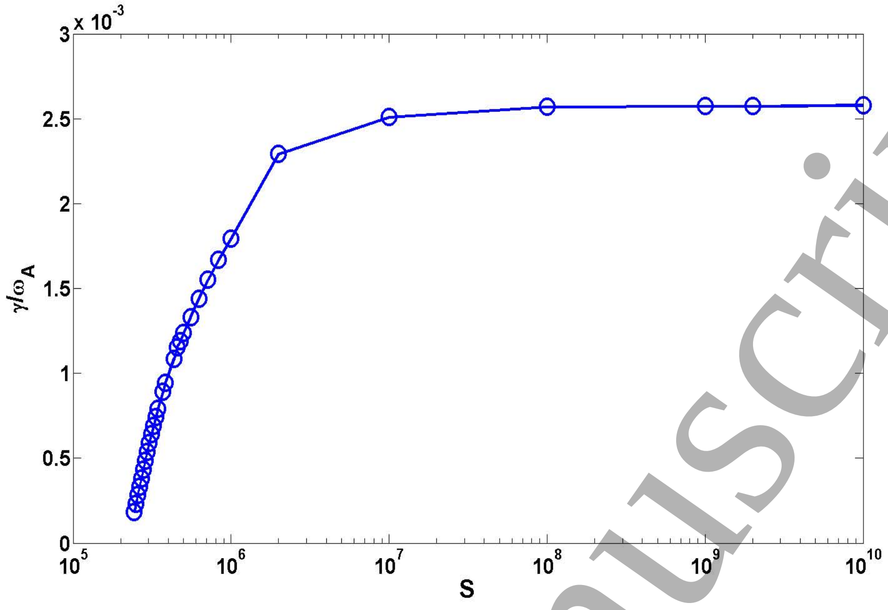

FIG. 10. Fishbone (a) growth rate and (b) real frequency as function of magnetic Reynolds number S. The equilibrium as case 4 in Fig. 3 and $\alpha_D = 0.3$ are adopted.

$d_e/r_1 < S^{-1/3} < \rho_s/r_1$. Hence, for the magnetic reconnection near the critical point of instability, the collisional resistivity is much more important than the electron inertial term [62], and the resistive-MHD model as used here is appropriate. Here, we scan S value from 2.5×10^5 to 10^{10} to study the effect of plasma resistivity on the fishbone as shown in Fig.10.

The plasma resistivity has a strong stabilization effect on fishbone near the marginal point ($\alpha_{(D,c)}$=0.22) when $S < 10^7$ (Fig.10). Mode growth rate reduces from 2.58×10^{-3} to 1.81×10^{-4} as the S changes from 10^7 to 2.5×10^5, in which $S^{1/3}\gamma/\omega_A <\sim 1$ being consistent with the results in Ref. [60, 61]. However, when the fishbone growth rate is large ($S^{1/3}\gamma/\omega_A > 1$), the resistivity effect is negligible. For the studied case (case 4 in Fig. 3), $S \sim 5 \times 10^7$ slightly enhances the threshold value from $\alpha_{D,c} \sim 0.22$ to ~ 0.23. It is pointed out that the Finite Larmor Radius (FLR) effect is not included in the model. However, FLR is an important effect to determine reconnection layer and qualitatively induces damping on fishbone onset [62]. Hence, FLR may further enhance the threshold value $\alpha_{D,c}$ for driving fishbone.

More interesting, the resistivity indeed affects the mode structure, including the plasma radial displacement and radial perturbed magnetic field as shown in Fig.11, as expected. The resistivity induces slight smoothing of the peaks (singularities) of imaginary part of $m = 1$ radial displacement (Fig.11(a)). Here, the singularities are induced by the resonance between precessional fishbone and shear Alfvén wave. For $m = 2$ poloidal harmonic, the resistivity clearly induces a tearing mode like structure, which implies a generation of reconnection at the $q = 2$ surface. Figure 11(c) indicates that the resistivity induces the finite m component of radial perturbed magnetic field at $q = m/n$ rational surface. While for the ideal case, the

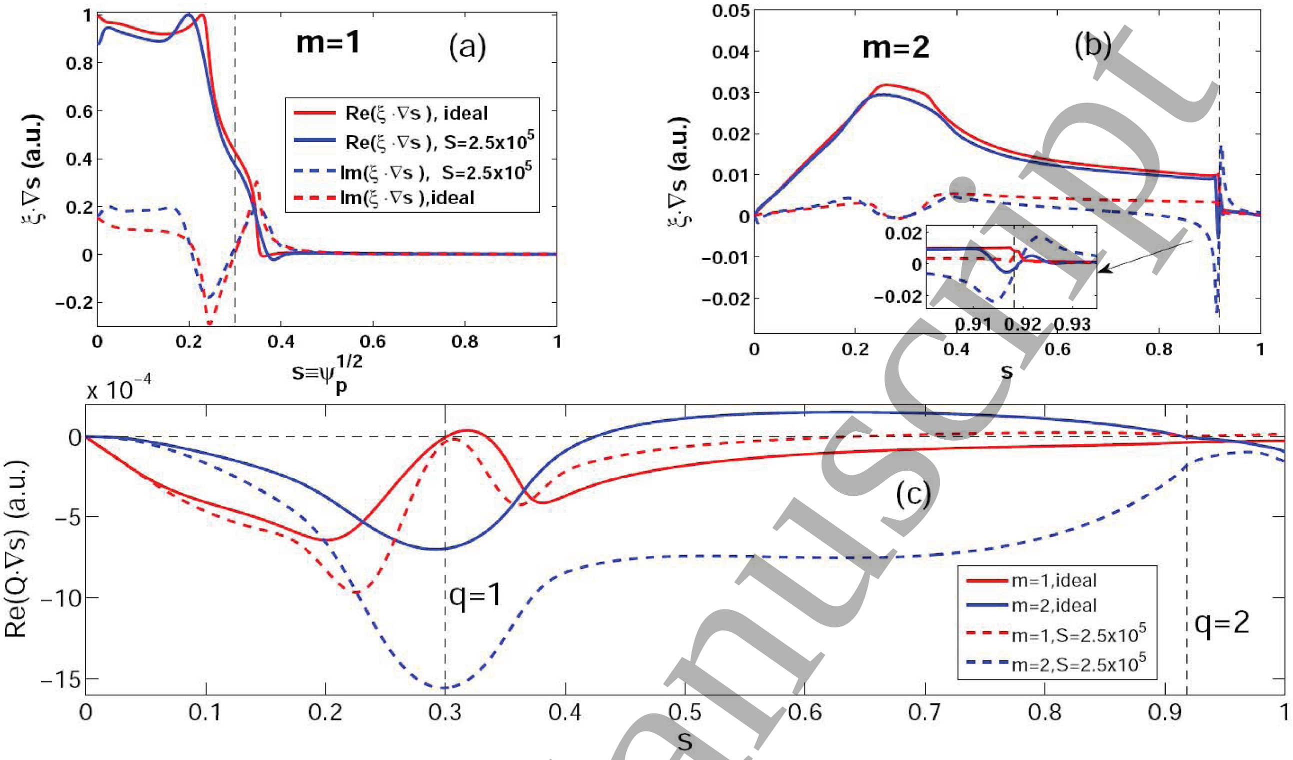

FIG. 11. The profiles of radial displacement for (a) $m = 1$ and (b) $m = 2$ harmonics. Here, for different harmonics, the maximum value of displacement components is normalized to unity, respectively. (c) shows the radial profile of real part of perturbed radial magnetic field for $m = 1$ and $m = 2$. Vertical lines denote the locations of rational surfaces.

radial perturbed field harmonic vanishes at the corresponding rational surface. It is implied that the $m/n = 1/1$ resistive fishbone or its higher harmonics can provide a seed island at an adjacent (e.g. $q = 2$) rational surface to initiate a reconnection.

However, the NTM initiated by fishbone may be related to not only the nonlinear interaction between resistive fishbone and continuum waves, but also the wave-particle nonlinearity as reviewed in Ref.[55]. It is still challenging to fully self-consistently nonlinear description of resistive fishbone, which also exceeds the scope of this work.

4. SUMMARY AND DISCUSSION

In this work, we apply MARS-K code to study the fishbone driven by trapped fast ions in a toroidal plasma, based on the non-perturbative approach. The influence of q profile, fast ion distribution, thermal ions and plasma resistivity on fishbone instability are investigated. The q profiles with very low and weakly reversed magnetic shear are considered in this work, as listed in table 1.

The main results are summarized below.

i. The fishbone in an equilibrium with $q_{min} > 1$ can be excited by isotropic or anisotropic

Table1. Details of q profiles used in this work

Type of *q* profile	Figures	Value of q minimum
reversed-shear	Figs.2, 6,7,8 and 9	0.97
	Fig.3	0.96, 1.01
	Fig.4	0.96
	Fig.5	from 0.92 to 1.1
monotonic	Figs.3, 4 ,10 and 11	0.947

fast ions, while the latter strongly enhances the mode. The mode frequency decreases as decreasing of q_{min}, which is a candidate explanation for the observed decrease of fishbone onset frequency in experiment as discussed in Ref.[55]. In addition, fishbone is much easier destabilised in an equilibrium with two $q = 1$ surfaces, compared with the case with one or without $q = 1$ surface. The possible reason may be that the resonance between the mode and particles increases with an increasing number of resonant surfaces.

ii. Kinetic contributions from transit resonance of passing fast ions and from bounce resonance of trapped fast ions strongly enhance the fishbone instability, due to the remarkable resonance between the mode and the above particles for the chosen fast ion distribution function. For the studied fishbone instabilities here, there is strong Landau damping induced by the transit resonance of passing thermal ions.

iii. Furthermore, in such a weak or even reversed magnetic shear plasma, the radial mode structure of the fishbone mode smoothly decreases to zero, without the abrupt transition layer at the $q = 1$ flux surface that is typical of a standard internal kink mode found at finite magnetic shear. Also, in our simulations, the radial displacement is found to depend self-consistently on the kinetic particle contributions. In theory, the modification of mode structure by particle kinetic effect is possibly caused by anti-Hermitian contributions due to wave-particle resonance [37]. As a consequence, while, for standard fishbones, one finds $-i\omega \propto -\delta W$, in our case $(-i\omega)^2 \propto -\delta W$.

iv. Plasma resistivity has a strong stabilization effect on the fishbone near the marginally unstable point (i.e. in the regime $S^{1/3}\gamma/\omega_A <\sim 1$). Plasma resistivity slightly affects the mode structure and results in the finite m component of radial perturbed field at $q = m/n$ surface, which may supply a seed island to initiate NTM.

Here, the used fast ion distribution function is relatively simple compared with the experimental one. In addition, here, we assumed that the birth energy of fast ions is about 45 keV in the whole region and ion temperature is about 1.5 keV at the axis. The change of fast ion birth energy and/or ion temperature may affect the strength of the thermal ion Landau damping. Landau damping depends on both the fishbone frequency and the passing thermal ion transit frequency in the studied case, which are related to the fast ion birth energy and ion temperature, respectively. In order to predict of thermal ion Landau damping on fishbone for the experiments, the realistic fast ion distribution and equilibrium profiles, including the thermal particle density and temperature profiles, should be used for the specific discharge.

It is noted that the self-consistent treatment of the fast ion kinetic effect on fishbone and internal kink was studied by NOVA-KN code. Some of our results are similar to those reported in Ref. [63]. For example, the trapped fast ion has a stabilization effect on internal kink, and drives a fishbone as fast ion pressure exceeds a threshold value. Fast ion kinetic effect has a modification effect on the fishbone mode structure. However, we present new results which are not reported in Ref. [63], such as the thermal ion effects on fishbone, dependence of fishbone on $q = 1$ surfaces and the effect of resistivity on fishbone as discussed in the text.

Fast ion transport induced by fishbone may depend on the mode structure. However, at present, an internal kink mode structure is often adopted to study the fast ion transport induced by fishbone instabilities [20–23]. It is interesting to study the sensitivity of the dependence of fast ion transport on the mode structure, which may have the contribution to build the reduced model to predict fast ion transport induced by fishbone instability.

We study the dependence of m/n=1/1 FB on the number of $q = 1$ surfaces and the magnetic shear in the core region. However, for the 9MA steady state ITER scenario, the q-profile has a wide weak shear region, and two $q = 2$ surfaces [2, 53]. The possibility of driving $n = 2$ fishbone-like instabilities in the reversed q-profile and its dependence on the q-profile are worthy to be investigated for the above ITER scenario.

5. ACKNOWLEDGMENTS

YTM and GZH thank Dr.Y.Q.Liu from General Atomics for his very valuable suggestions and encouragements. Authors thank the anonymous referees for the constructive comments and helpful suggestions. This work was supported by the National Natural Science Foundation of China under Grant No. 11775067, 11905067 and also supported by National Magnetic Confinement Fusion Science Program under Grant Nos. 2018YFE0304103 and 2015GB104004.

[1] G. Z. Hao *et al.*, Phys. Rev. Lett. **107**, 015001 (2011).
[2] Y. Q. Liu *et al.*, Phys. Plasmas **21**, 056105 (2014).
[3] Y. Q. Liu, Nucl. Fusion **50**, 095008 (2010).
[4] H. S. Cai *et al.*, Phys. Rev. Lett. **106**, 075002 (2011).
[5] L. Chen *et al.*, Rev. Mod. Phys. **88**, 015008 (2016).
[6] G. Y. Fu *et al.*, Phys. Fluids B **5**, 4040 (1993).
[7] L. Chen *et al.*, Phys. Rev. Lett. **52**, 1122 (1984).
[8] B. Coppi *et al.*, Phys. Rev. Lett. **57**, 2272 (1986).
[9] S. C. Guo *et al.*, Nucl. Fusion **56**, 056006 (2016).

[10] G. Z. Hao *et al.*, Phys. Plasmas **19**, 2709 (2012).

[11] G. Z. Hao *et al.*, Phys. Plasmas **20**, 87 (2013).

[12] K. McGuire *et al.*, Phys. Rev. Lett. **50**, 891 (1983).

[13] W. W. Heidbrink *et al.*, Phys. Rev. Lett. **57**, 835 (1986).

[14] W. W. Heidbrink *et al.*, Nucl. Fusion **34**, 535 (1994).

[15] W. W. Heidbrink *et al.*, Nucl. Fusion **52**, 094005 (2012).

[16] K. L. Wong *et al.*, Phys. Rev. Lett. **85**, 996 (2000).

[17] M. F. F. Nave *et al.*, Nucl. Fusion **31**, 697 (1991).

[18] D. Borba *et al.*, Nucl. Fusion **40**, 775 (2000).

[19] F. Nabais *et al.*, Phys. Plasmas **12**, 102509 (2005).

[20] C. Perez von Thun *et al.*, Nucl. Fusion **50**, 084009 (2010).

[21] C. Perez von Thun *et al.*, Nucl. Fusion **51**, 053003 (2011).

[22] C. Perez von Thun *et al.*, Nucl. Fusion **52**, 094010 (2012).

[23] M. Fitzgerald *et al.*, Nucl. Fusion **59**, 016004 (2019).

[24] V. Kiptily *et al.*, Nuclear Fusion **58**, 014003 (2018).

[25] G. Matsunaga *et al.*, Phys. Rev. Lett. **103**, 045001 (2009).

[26] L. Q. Xu *et al.*, Phys. Plasmas **22**, 122510 (2015).

[27] W. Chen *et al.*, Nucl. Fusion **49**, 075022 (2009).

[28] W. Chen *et al.*, Nucl. Fusion **50**, 084008 (2010).

[29] M. Jiang *et al.*, Phys. Plasmas **24**, 022110 (2017).

[30] E. Fredrickson *et al.*, Nucl. Fusion **43**, 1258 (2003).

[31] I. T. Chapman *et al.*, Nuclear Fusion **51**, 073040 (2011).

[32] R. B. White *et al.*, Phys. Fluids **26**, 2958 (1983).

[33] L. M. Yu *et al.*, Nucl. Fusion **59**, 086016 (2019).

[34] F. Wang *et al.*, Nucl. Fusion **57**, 056013 (2017).

[35] R. Betti *et al.*, Phys. Rev. Lett. **70**, 3428 (1993).

[36] B. J. Tobias *et al.*, Phys. Rev. Lett. **106**, 075003 (2011).

[37] R. R. Ma *et al.*, Phys. Plasmas **22**, 092501 (2015).

[38] Y. R. Yang *et al.*, Plasma Sci. Technol **21**, 85101 (2019).

[39] J. E. Menard *et al.*, Nucl. Fusion **45**, 539 (2005).

[40] Z. Z. Ren *et al.*, Phys. Plasmas **25**, 122504 (2018).

[41] Y. Q. Liu *et al.*, Phys. Plasmas **15**, 112503 (2008).

[42] J. W. Berkery *et al.*, Phys. Plasmas **21**, 052505 (2014).

[43] F. Porcelli *et al.*, Phys. Plasmas **1**, 470 (1994).

[44] N. N. Gorelenkov *et al.*, Nucl. Fusion **45**, 226 (2005).

[45] M. Xu *et al.*, Nucl. Fusion **59**, 112017 (2019).

[46] S. X. Yang *et al.*, Nucl. Fusion **58**, 046016 (2018).

[47] S. X. Yang *et al.*, Phys. Plasmas **22**, S128 (2015).

[48] R. J. Hastie *et al.*, Phys. Fluids **30**, 1756 (1987).

[49] I. T. Chapman *et al.*, Nucl. Fusion **50**, 045007 (2010).

[50] L. M. Yu *et al.*, Nucl. Fusion **57**, 036023 (2017).

[51] A. Kirk *et al.*, Nucl. Fusion **57**, 102007 (2017).

[52] J. E. Menard *et al.*, Phys. Rev. Lett. **97**, 095002 (2006).

[53] T. Casper and A. Polevoi, ITER Documentation , No. 2V3FDF (2009).

[54] M. N. Bussac *et al.*, Phys. Rev. Lett. **35**, 1638 (1975).

[55] B. N. Breizman and S. E. Sharapov, Plasma Phys. Control. Fusion **53**, 054001 (2011).

[56] F. Wang *et al.*, Phys. Plasmas **20**, 102506 (2013).

[57] X. Q. Wang *et al.*, Plasma Phys. Controlled Fusion **56**, 095013 (2014).

[58] W. Chen *et al.*, Nucl. Fusion **58**, 014001 (2018).

[59] A. Gude *et al.*, Nucl. Fusion **39**, 127 (1999).

[60] H. Biglari and L. Chen, Phys. Fluids **29**, 1760 (1986).

[61] T. T. Wu *et al.*, Phys. Plasmas **25**, 052504 (2018).

[62] F. Porcelli *et al.*, Plasma Phys. Control. Fusion **38**, 2163 (1996).

[63] N. N. Gorelenkov *et al.*, 20th IAEA-FEC Conference, Vilamoura, Portugal,1st-6th,November (2004).